Pergamon

PII: S0042-6989(96)00250-7

Vision Res., Vol. 37, No. 9, pp. 1141–1155, 1997

Printed in Great Britain
0042-6989/97 $17.00 + 0.00

Comparison between Spatial Interactions in Perceived Contrast and Perceived Brightness

JEREMY S. DE BONET,* QASIM ZAIDI†‡

Received 6 December 1995; in revised form 18 July 1996; in final form 19 August 1996

We examined the spatial integration of simultaneously induced achromatic contrast and compared it to the spatial integration of simultaneously induced brightness. This study extends the work of Zaidi *et al.* [(1992). *Vision Research, 32*, pp. 1695–1707], who showed that the total magnitude of induced brightness can be described as the weighted sum of the brightness induced by individual elements of the surround. The results show that contrast induction, though weaker than brightness induction, occurs over greater distances, and that a weighted spatial summation model for contrast induction requires an additional static non-linear compression, which is not required to model brightness induction. The analysis indicates that the contrast compression occurs prior to the lateral interactions that generate induced contrast. © 1997 Elsevier Science Ltd. All rights reserved.

Contrast Brightness Lateral interactions Spatial integration Induction

INTRODUCTION

The appearance of an area of visual space is affected in a complex manner by surrounding areas. The perceived color, brightness, size, depth, form, motion, surface mode, etc., can be modified by changing the relative value of the same, and in some cases different, perceptual dimensions in the surround (Zaidi and Sachtler, 1991; Adelson, 1993; Zaidi *et al.*, 1996). The ubiquity of surround effects makes it important to study the organization of lateral interactions between neural elements at various stages of the visual system. Psychophysical experiments can contribute to this analysis by separating the effect of the relative intensity of the relevant quality from the effect of the spatial arrangement. In this study we attempt to provide a punctate level account of the lateral interactions involved in perceived achromatic contrast.

When a test patch containing random texture is surrounded by random texture of similar grain, the perceived contrast within the test is a function of both the physical contrast in the test and the difference in contrast between the test and the surround. When two such textured patches are juxtaposed, there is an increase in the perceived difference between their contrasts. By analogy to classical induced brightness (or color) contrast (Chevreul, 1839), this phenomenon was termed induced contrast-contrast by Chubb *et al.* (1989). Ejima and Takahashi (1985) reported similar lateral effects using gratings.

For induced achromatic brightness, Zaidi *et al.* (1992) showed that the total effect of the surround could be described as the sum of the induced effects of individual elements of the surround, where the effects of different surround elements of the same amplitude were a monotonically decreasing function of distance from the test. The spatial summation inference was based on the results of superposition tests, i.e., the induced effect of every pair of surrounds presented simultaneously was equal to the sum of the induced effect of each component presented singly. Because brightness induction passed superposition tests, we were able to use a linear spatial summation model to estimate the nonlinear spatial weighting function. The failure of a superposition test, however, can still be consistent with linear spatial summation if the failure is due to an amplitude non-linearity, which can be identified directly by measuring the magnitude of induction at scalar multiples of the amplitude of the surround.

The purpose of the present study was to apply a similar analysis to induced achromatic contrast, i.e., to examine the spatial combination rule and to estimate the spatial weighting function. We present the results of four experiments. In Experiment 1 we measured the magnitude of induction due to surrounds whose contrast or brightness was varied sinusoidally with increased distance from the test. Using linear systems methods, the results of Experiment 1 could be used to estimate the effective weight of elements in the surrounds at increasing distances from the test. In Experiment 2, the

*M.I.T., Artificial Intelligence Laboratory, 545 Technology Square, Cambridge, MA 02139, U.S.A.

†S.U.N.Y. College of Optometry, 100 East 24th St, New York, NY 10010, U.S.A.

‡To whom all correspondence should be addressed [*Fax* +1-212-780-5009; *Email* qz@wotan.cns.nyu.edu].

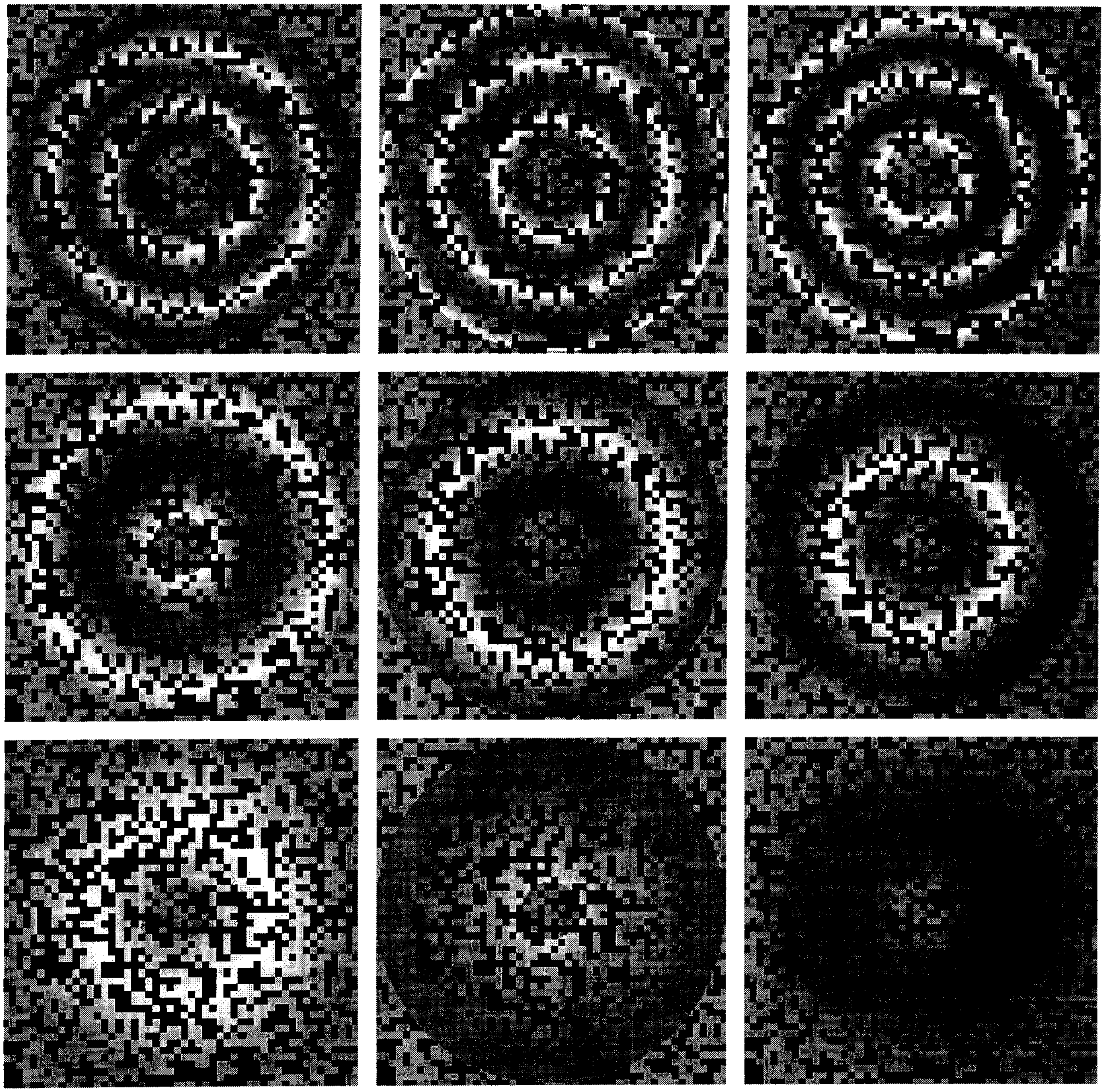

FIGURE 1. Single frequency contrast induction stimuli. Surrounds are composed of binary random texture whose contrast varies sinusoidally along each radius. Each row depicts one spatial frequency condition. Across each row, the surround is shown at three different phases. The central disks are the tests, and have the same texture as the surround. In all nine pictures the tests are at 50% contrast; different apparent contrasts are due to different amounts of induced contrast from the surround.

spatial superposition assumption for such linear systems was tested, using surrounds composed of sums of sinusoids of different frequencies. In Experiment 3, the scalar multiplication assumption was tested by varying the amplitude of modulation in the surround. In Experiment 4, we used the more traditional technique of varying the surround size to test the weighted spatial summation model. In all four of these experiments, the effects of similar spatial and temporal variations of achromatic contrast and achromatic brightness were studied for each observer. The experiments and models in this study dealt with spatial variations in contrast or brightness at a punctate level. The results provide information about the fine structure of lateral interactions involved in contrast and brightness perception.

EXPERIMENT 1: INDUCTION FROM SIMPLE CIRCULAR SINUSOIDAL SURROUNDS

The contrast induction effects of the surround at varying distances from the test were studied using stimuli similar to those shown in Fig. 1. The central disks are the test regions. The test and surround are composed of uniformly distributed binary random texture of identical frequency. In the surround the contrast within the carrier noise is varied along each radial direction, resulting in a blurred bullseye target whose concentric rings vary sinusoidally from 0% contrast (uniform gray rings) to 100% contrast (black and white textured rings). Both the space-averaged contrast and luminance are fixed at the mean level. Contrast for each concentric ring is defined as the standard Michelson contrast: $(L_{max} - L_{min})/(L_{max} + L_{min})$, where L_{max} and L_{min} are the luminance of the light and dark texture elements, respectively; within each ring $L_{min} + L_{max} = 1$. The uniform distribution of light and dark texture elements assures that the average luminance of each ring is equal to the mean level of the display. The central disks in all nine pictures are at the mean contrast level. Each of the rows of Fig. 1 shows the contrast varying surrounds of a single spatial frequency that were used in a single condition. Each row shows three spatial phases of the contrast sine wave. In this paper we will refer to the spatial frequency of the contrast modulation as the spatial frequency of the surround; the size of the squares in the random texture affects only the carrier frequency. Two aspects of the phenomenal appearance of the central test are directly relevant to the present study. First, within each row, as the phase of the surrounding sine-wave changes, the appearance of the test changes. The apparent contrast in the test is roughly inversely proportional to the apparent contrast of the inner edge of the surround. Each row actually illustrates three phases of

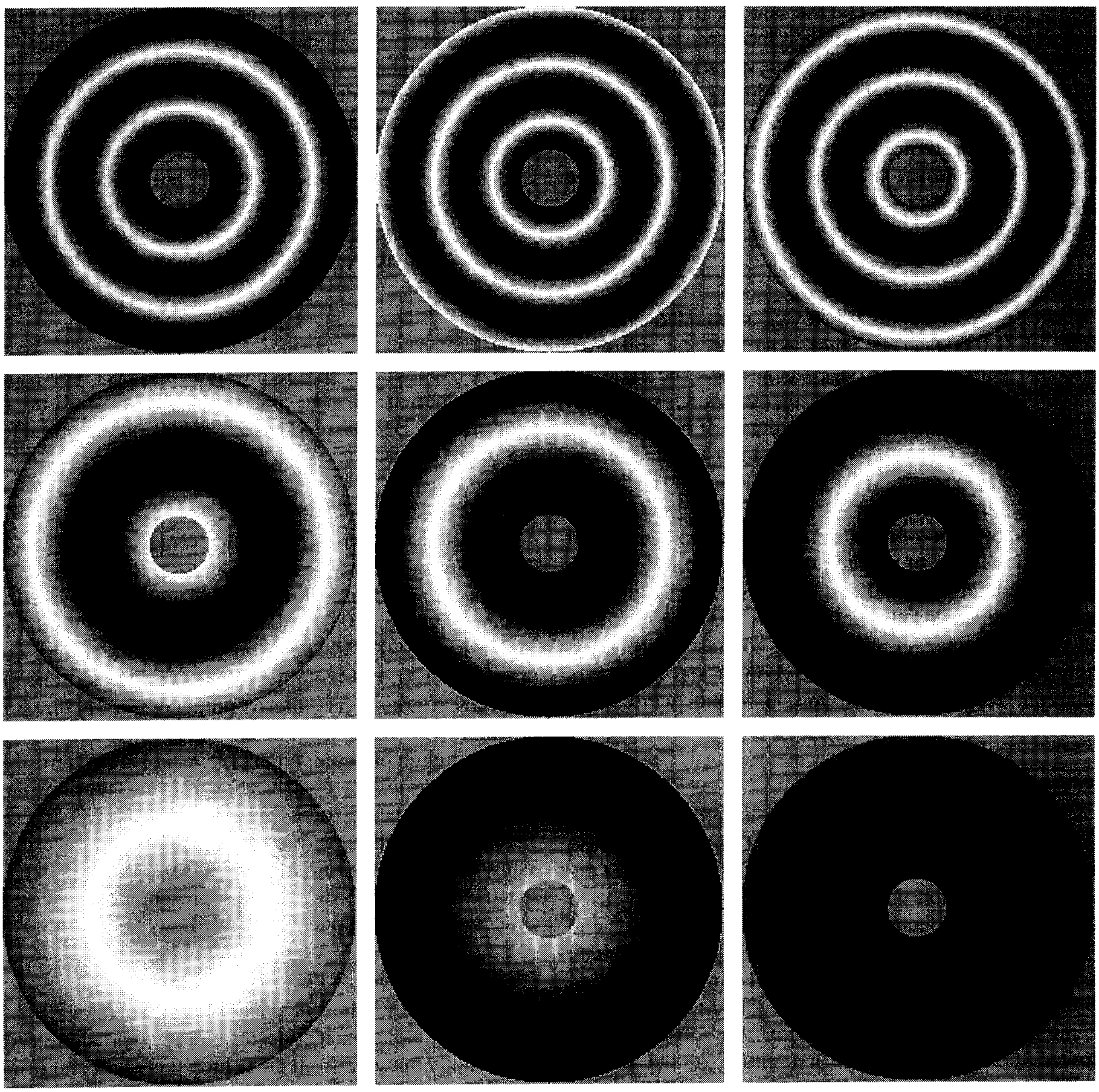

FIGURE 2. Single frequency brightness induction stimuli. Surrounds are spatially uniform annuli whose luminance varies sinusoidally along each radius. Each row depicts one spatial frequency condition. Across each row, the surround is shown at three different phases. The central disks are the tests, and in all nine pictures are at the same mid-gray luminance; the differences in apparent brightnesses are due to different amounts of induced brightness from the surround.

the temporal modulation used in the first experiment. The surround consisted of a single sine-wave of one of eight different spatial frequencies. As the phase of the surround (with respect to the inner edge) was changed uniformly in time, so that the sine-wave appeared to drift toward the center at a constant velocity, the appearance of the central test changed cyclically in time. Second, the magnitude of the change in apparent contrast is least in the top row, which has the surround with the highest spatial frequency, and greatest in the bottom row, which has the surround with the lowest spatial frequency.

Using a set of stimuli identical to those used by Zaidi *et al.* (1992), we also measured the brightness induction effects of the surround in a manner that permits a comparison to the contrast induction effects. These stimuli, shown in Fig. 2, use the same spatial configurations as were used for the contrast induction experiment, except that sinusoidal luminance variation has been substituted for sinusoidal contrast variation. The central tests are all at the same mean luminance level. Figure 2 demonstrates brightness phenomena that can be compared to the contrast induction shown in Fig. 1. The apparent brightness of the central disk varies with both the spatial frequency and phase of the surround.

Stimulus parameters

The test, centered on the fovea, subtended a visual angle of 1.0 deg. The inner edge of the surround coincided with the outer edge of the test. The diameter of the circular outer edge of the surround subtended 9.5 deg of visual angle. The magnitude of both contrast and brightness induction were measured for sine-waves with spatial frequencies (along radial lines) of 0.03, 0.06, 0.125, 0.25, 0.5, 1.0, 2.0 or 4.0 c/deg. The sine-wave was drifted inside the window towards the center at a speed of 0.5 Hz. In the case of contrast induction, the size of each square element was 0.1 deg on a side. The circular surround was enclosed within a 9.5×13.0 deg rectangle that was held constant at the mean contrast or the mean brightness level, in the cases of contrast and brightness induction, respectively. All measurements were made with centrally fixated binocular viewing.

Measurement procedure

A 2AFC version of the modulation nulling technique discussed by Krauskopf *et al.* (1986), Chubb *et al.* (1989) and Zaidi *et al.* (1991, 1992), was used to measure the amount of induction within the central test. During each trial, the observer fixated on the test. When the surround components were drifted inwards at 0.5 Hz, a perceived modulation was induced in the test. To null the induced modulation, a real modulation was added to the test. As an initial step for each condition, the observer was allowed to freely adjust the magnitude of the nulling modulation to minimize the perceived modulation in the test. This setting was used to initialize a pair of staircases, 24% above and below the setting. Different tones were presented simultaneously with the positive and negative peaks of each sinusoidal cycle. During the 2AFC portion of the procedure, the observer's task was to compare the test appearances at the two tones, and to respond whether the apparent contrast (or brightness) of the test at the second tone was higher or lower than at the first tone by pressing the appropriate buttons. From this response it was determined whether the nulling modulation was stronger or weaker than the induced modulation. When the observer's response indicated that the nulling modulation was stronger (or weaker) than the induced modulation, nulling modulation was reduced (or increased) by 12%. A turn in the staircase occurred when the observer's response indicated that the nulling modulation had changed from weaker to stronger than the induced modulation (or vice versa). Each of these turns is an estimate of the observer's required nulling modulation, and the staircases continued until 10 such turns had been accumulated. To ensure the reliability of the measurements we extracted several statistics. By examining the standard deviation we confirmed that each staircase converged; and by examining the *t*-test and F-Ratio, we confirmed that the two staircases converged on the same value, despite having been initialized at different points. During each session the observer was presented with randomly interleaved conditions to insure that adaptation to a particular surround modulation would not occur.

Observers

One experienced psychophysical observer (BS) and one inexperienced observer (AR) participated in all experiments. Both observers were corrected to normal for refractive errors.

Equipment and calibration

Stimuli were displayed on the screen of a BARCO 7651 color monitor with a refresh rate of 100 frames/sec. Images were generated using a Cambridge Research Systems Video Stimulus Generator (CRS VSG2/2), running in a 90 MHz Pentium based system. Through the use of 12-bit DACs, the VSG2/2 is able to generate 2861 linear gray levels after gamma correction, any 256 of which can be displayed during a single frame. By cycling though pre-computed look up tables we were able to update the entire display each frame. The phosphor chromaticity specifications supplied by BARCO and the gamma-corrected linearities of the guns were verified using a Spectra Research Spectra-Scan PR-650 Photo-spectroradiometer. All stimulus presentation and data collection were computer controlled.

The binary random texture stimulus

Each binary random dot pattern was arranged so that on average, along each concentric circle, and along each line radially outward from the center, there was a uniform distribution of the two texture elements. Stimuli were generated so that the contrast between the texture elements along each concentric circle could be independently controlled. This allowed for a wide range of frequencies of the spatial sinusoidal variation. It is

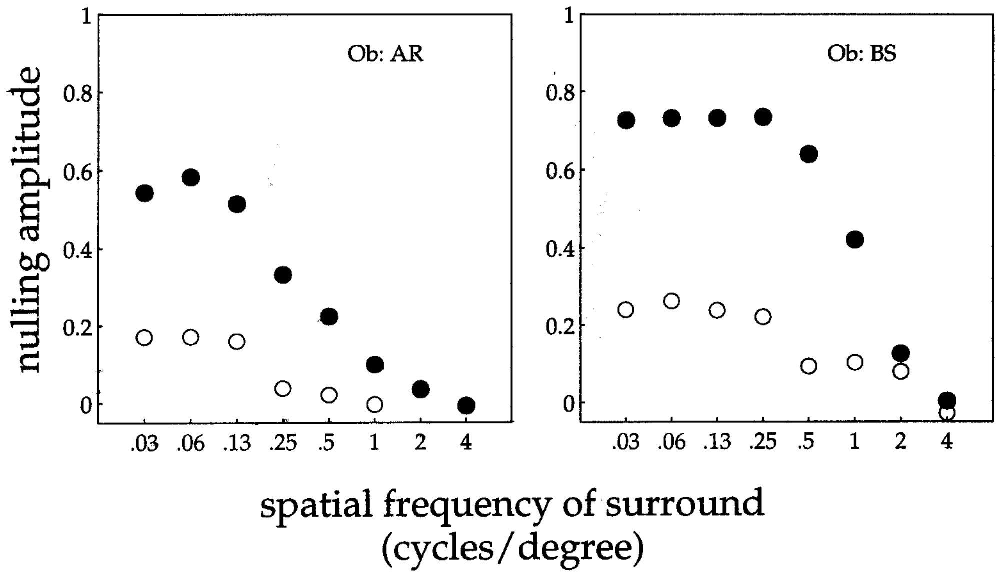

FIGURE 3. Results of Experiment 1 for two observers. The amplitude of modulation required to null induction is plotted against the spatial frequency of the surrounding contrast sine-wave. Open symbols are contrast and filled symbols are brightness induction nulls. Each data point is the average of two 2AFC staircases (10 turns each). Error bars representing standard error of the mean were smaller than the symbols.

important to note that the luminance of each texture element was not uniform but varied smoothly, allowing the sinusoidal contrast drift to be smooth and independent of texture size.

Results

The contrast and brightness induction results for both observers are shown in Fig. 3. The contrast modulation (open symbols) and brightness modulation (closed symbols) required to null the induced modulation are plotted vs the spatial frequency of the surround modulation on a logarithmic scale. Each point in these graphs is the mean of 20 transition points from two independent staircases. Error bars indicating the standard error of the mean were smaller than the symbols. For both observers both contrast and brightness induction are low-pass functions of surround spatial frequency. The required nulling magnitudes indicate that contrast induction is a weaker effect than brightness induction, by a factor of two to three.

If we assume a weighted spatial summation model such as that proposed by Zaidi *et al.* (1992), i.e., that the net induced effect is the weighted summation of the inducing effect of each point in the surround, then the above data predict a spatial weighting function that can be closely approximated by a negative exponential function. Further, when plotted on a log–log scale, the contrast induction data yield a narrower curve than brightness induction. Therefore its Fourier transform though weaker in absolute magnitude, predicts a larger area of summation in contrast induction, than for brightness induction. This would indicate that the lateral interactions affecting perceived contrast occur over a greater distance than do those affecting perceived brightness.

EXPERIMENT 2: INDUCTION FROM COMPOUND SINUSOIDAL SURROUNDS

The spatial superposition assumption required for the analysis described above was tested by comparing the induced effect of surrounds composed of pairs of circularly symmetric sine-waves to the sum of the induced effects of the constituent sine-waves. The paired sine-waves were set to be in identical phase at the inner edge of the surround. These compound stimuli are shown varying in contrast and luminance in Figs 4 and 5, respectively. The central disks are the test regions. In Fig. 4 the test regions are at the mean contrast level, and in Fig. 5 they are at the mean luminance level. Each row shows surrounds consisting of the sum of two spatial frequencies windowed by the edges of the surround. The three rows consist of the same medium frequency paired with a high (top row), medium (middle row), and low frequency (bottom row). Across each row in Figs 4 and 5, three phases (with respect to the inner edge) of the paired sine waves are shown. Though the central disks are all at the same contrast (Fig. 4) or luminance level (Fig. 5), they appear to be different, depending on the frequencies and phase of the surrounding sine-waves. Sine-waves of each of the eight spatial frequencies used in Experiment 1 were paired with each other, yielding 64 compound surrounds. The amplitude of each constituent sine-wave was 0.5 to give a maximum amplitude modulation of 1.0.

Results

Figures 6 and 7 show the data for the 64 paired contrast sine-waves and the 64 paired luminance sine-waves, respectively. Each point is the mean of 20 transition points from two independent ten-transition staircases. The ordinate of each point is the amplitude of the

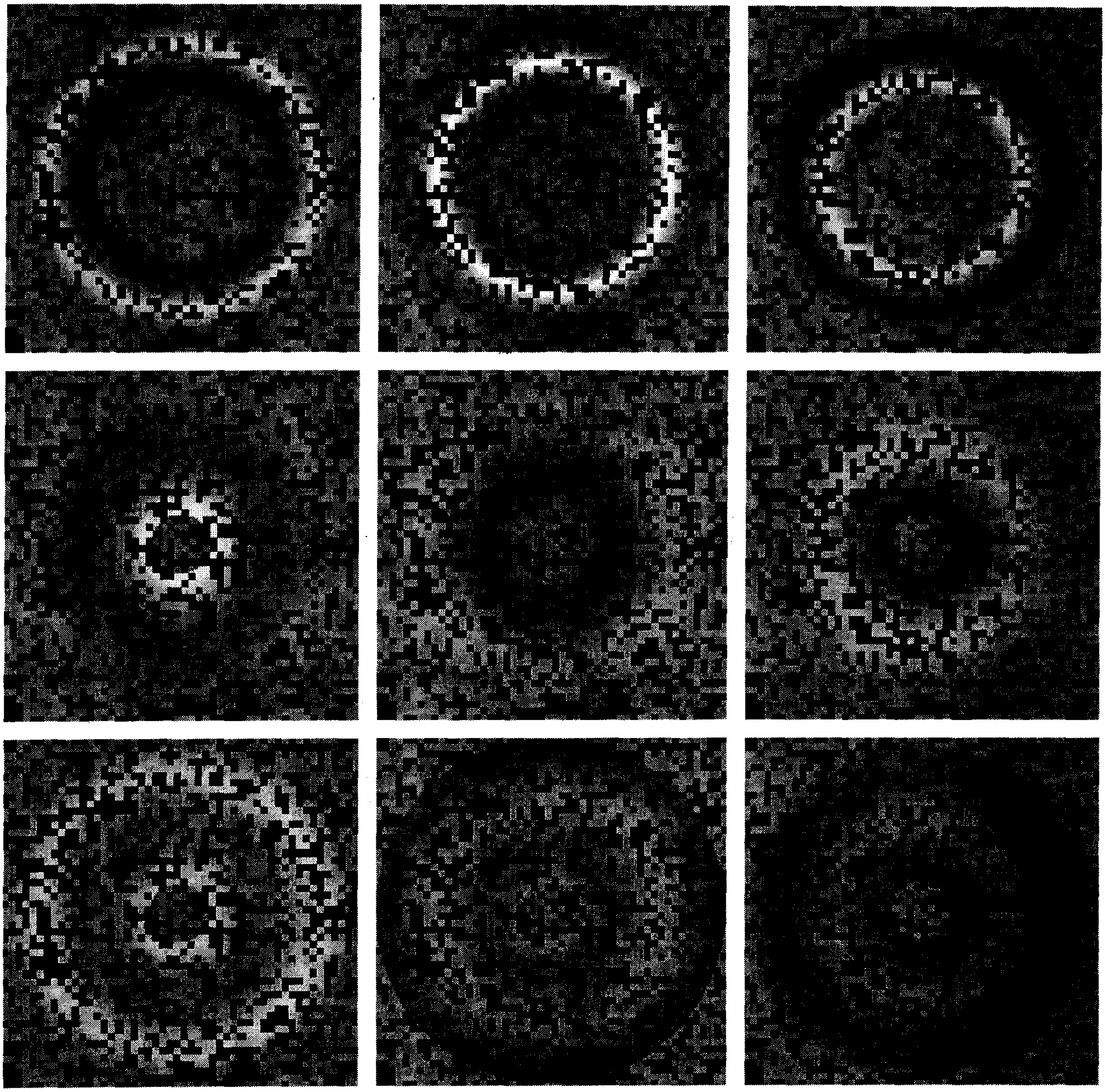

FIGURE 4. Compound frequency contrast induction stimuli. Surrounds are composed of binary random texture whose contrast varies as the sum of two sine-waves of different frequencies along each radius. The top row shows a high frequency sine-wave added to a medium frequency sine-wave; middle row, two different intermediate frequency sine-waves are added; bottom row, a low frequency sine-wave is added to a medium frequency sine-wave. Across each row, the surround is shown at three different phases. The central disks are the tests, and have the same texture as the surround. In all nine pictures the tests are at 50% contrast; different apparent contrasts are due to different amounts of induced contrast from the surround.

required nulling modulation. Each curve in the figures connects the data for a particular spatial frequency, when paired with the spatial frequencies corresponding to the abscissa. Different line types have been used to distinguish the curves. The key to identifying the curves is to begin at the leftmost point, where the curves are ordered from top to bottom in the same order as the spatial frequencies shown in the caption.

All the curves for brightness induction (Fig. 7) are roughly parallel and have similar shapes, indicating that the amount of modulation required to null the induced effect decreases as each frequency is paired with progressively higher frequencies. Additionally, the incremental induced effect of adding sine-waves of different spatial frequencies (represented by the curves) is fairly independent of the paired spatial frequency (indicated on the abscissa). Because summation holds, a punctate summation model can be used to fit the brightness induction data.

On the other hand, the curves for contrast induction

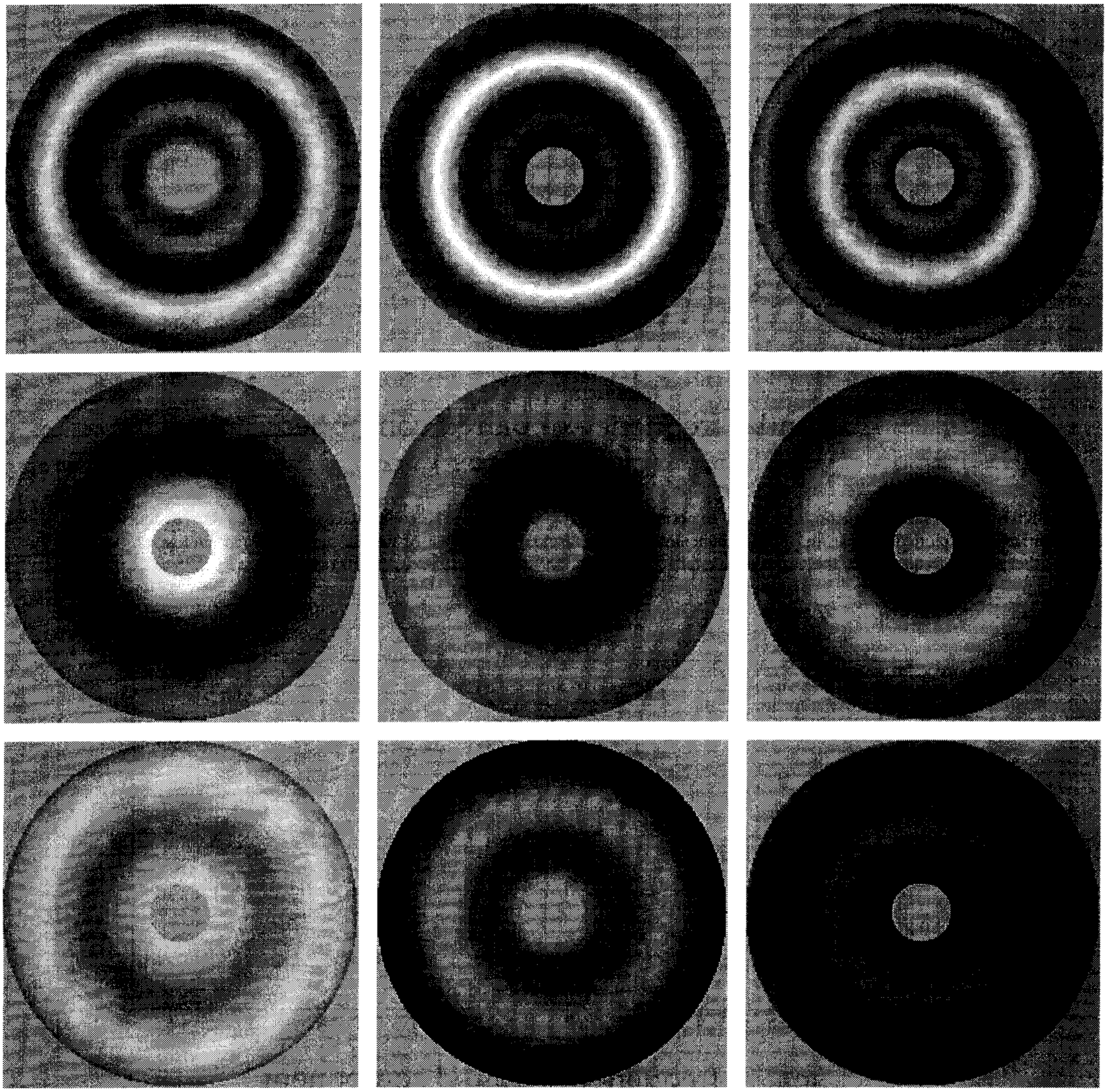

FIGURE 5. Compound frequency brightness induction stimuli. Surrounds are spatially uniform annuli whose luminance varies as the sum of two sine waves of different frequencies along each radius. The top row shows a high frequency sine-wave added to a medium frequency sine-wave; middle row, two different intermediate frequency sine-waves are added; bottom row, a low frequency sine-wave is added to a medium frequency sine-wave. Across each row, the surround is shown at three different phases. The central disks are the tests, and in all nine pictures are at the same mid-gray luminance; different apparent brightnesses are due to different amounts of induced brightness from the surround.

(Fig. 6) are not parallel. The range covered by the left-hand side of the curves (pairs which include the lowest spatial frequency) is considerably less than the range covered by the right-hand side (pairs which include the highest spatial frequency). However, this may not be irreconcilable with spatial summation if the non-linearity in the data is due simply to amplitude non-linearities in contrast induction.

EXPERIMENT 3: INDUCTION FROM SURROUNDS MODULATED WITH DIFFERENT AMPLITUDES

To model contrast and brightness induction as linear systems it is necessary that the amplitude of nulling modulation be a linear function of the amplitude of inducing modulation. The purpose of Experiment 3 was to test this. We measured the amplitude of the induced modulation generated by surrounds with a spatial

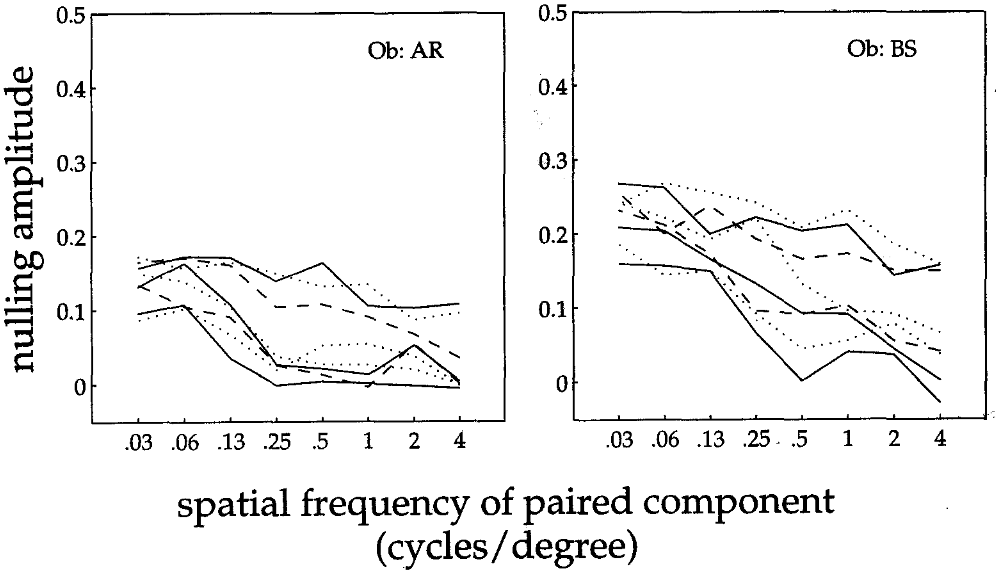

FIGURE 6. Contrast induction results of Experiment 2 for two observers. The contrast modulation required to null contrast induction is plotted against the spatial frequency of one sinusoidal component of the surrounding compound wave, with the other spatial frequency as the curve parameter indicated by the line types: 0.03 ——, 0.06 ....., 0.13 – –, 0.25 ——, 0.50 ...., 1.00 – –, 2.00 ——, 4.00 .....

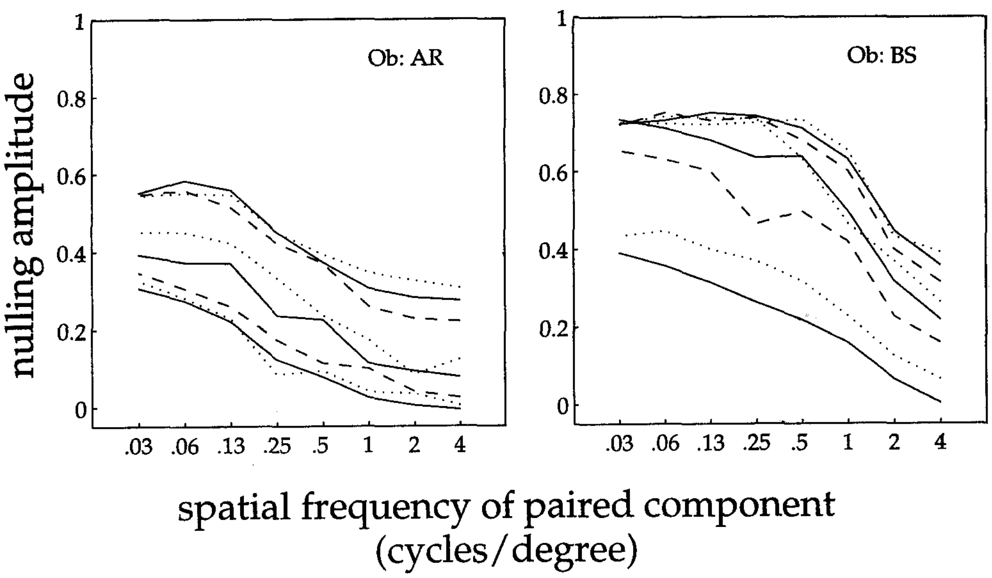

FIGURE 7. Brightness induction results of Experiment 2 for two observers. The luminance modulation required to null brightness induction is plotted against the spatial frequency of one sinusoidal component of the surrounding compound wave, with the other spatial frequency as the curve parameter indicated by the line types: 0.03 ——, 0.06 ....., 0.13 – –, 0.25 ——, 0.50 ....., 1.00 – –, 2.00 ——, 4.00 .....

frequency of zero, modulated with different amplitudes. The departure of these nulls from a linear function of inducing amplitude would indicate amplitude non-linearities in the relevant mechanisms. Induction levels were measured for contrast and brightness configurations with amplitudes of modulation ranging from 0.0 to 1.0, in 0.1 increments.

Results

The results are shown for both observers in Fig. 8. In the contrast induction series (open symbols) for both observers the points form a compressive non-linear curve. For both observers, the brightness induction amplitude series (filled symbols) is fairly close to linear.

R^2s were calculated for the best-fitting straight line and the best-fitting odd symmetric polynomial of the form:

$$N(A) = m(A - cA^3) \tag{1}$$

where N is the required nulling modulation and A is the surround modulation amplitude. We used the coefficient

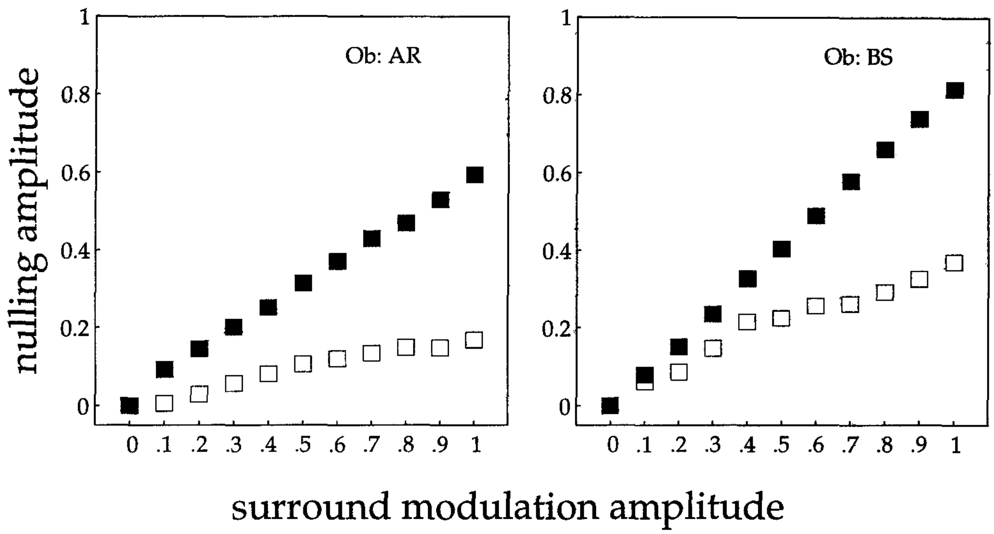

FIGURE 8. Results of Experiment 3 for two observers. The contrast or luminance modulation required to null contrast or brightness induction plotted against the amplitude of surround modulation. Open symbols are contrast and filled symbols are brightness induction nulls.

c as a metric of compression. For the contrast series, the polynomial fit was significantly better than the linear fit for both observers. R^2 improved from 0.9692 to 0.9845 for AR ($c = 0.20$) and from 0.9415 to 0.9761 for BS ($c = 0.26$). For BS, the best-fitting polynomial to the brightness series was the same as the best linear fit, with R^2 equal to 0.9995 ($c = 0$). For AR, the best fit to the brightness series had a small amount of compression ($c = 0.10$), but the compression was a non-significant improvement over the linear fit with R^2 equal to 0.9957 vs 0.9918. In a later section, we will use the contrast induction amplitude non-linearity to extend the linear point-wise summation model.

EXPERIMENT 4: INDUCTION FROM UNIFORMLY MODULATING SURROUNDS OF VARYING DIAMETER

The effect of distance on induction level was also measured using a more traditional method, by varying the size of the modulating surround annulus. Using both contrast and brightness configurations, we measured the amplitude of the modulation required to null the induction generated by uniform modulation of surrounds with outer diameters of 2.4, 3.2, 4.8, 7.3, and 9.5 deg. The inner edge of all surrounds coincided with the outer edge of the test (diameter of 1.0 deg).

Results

Figure 9 shows the results for contrast (open symbols) and brightness induction (filled symbols), for two observers. Required nulls are plotted as functions of the outer diameter of the modulating surround. Each data point is the mean of twenty measurements and error bars indicating the standard error of the mean fall within the symbols. For both observers, contrast and brightness induction levels increase with an increase in the size of the surround. In all cases the level of induction reaches an asymptote, indicating diminishing contributions to the total induced modulation from elements of the surround at increasing distances from the test. These results will be used to test the generality of the model that is fit to the results of the first three experiments.

WEIGHTED SPATIAL INTEGRATION MODEL OF INDUCTION

The results of brightness induction have previously been interpreted in terms of a simple model that postulates a weighted spatial integration of induced effects (Zaidi *et al.*, 1992; Spehar *et al.*, 1996). The perceived brightness at a point in visual space has two components, one due to the luminance of the light emanating from that point and the second due to the total induced effect of surrounding points. The model makes three assumptions about the induced effect. First, the induced effect of any surrounding point is in the complementary direction from the surround luminance relative to the test, with a magnitude proportional to the difference between the surround point and the mean level of the whole surround. Second, the induced effect of each surrounding point is weighted by a decreasing function of spatial distance from the test point. Third, the total induced effect is simply the sum of the induced effects of individual surrounding points. Algebraically, this model is defined by equation (2):

$$y = -\int_0^{2\pi} \frac{\int_0^{\infty} g(\Omega, s)A(\Omega, s)s\,ds}{2\pi}\,d\Omega \qquad (2)$$

where y is the total induced effect at the test point, Ω is the angular orientation, and s is the spatial distance between the test and induction point, $g(\Omega,s)$ is the monotonically decreasing spatial weighting function of s,

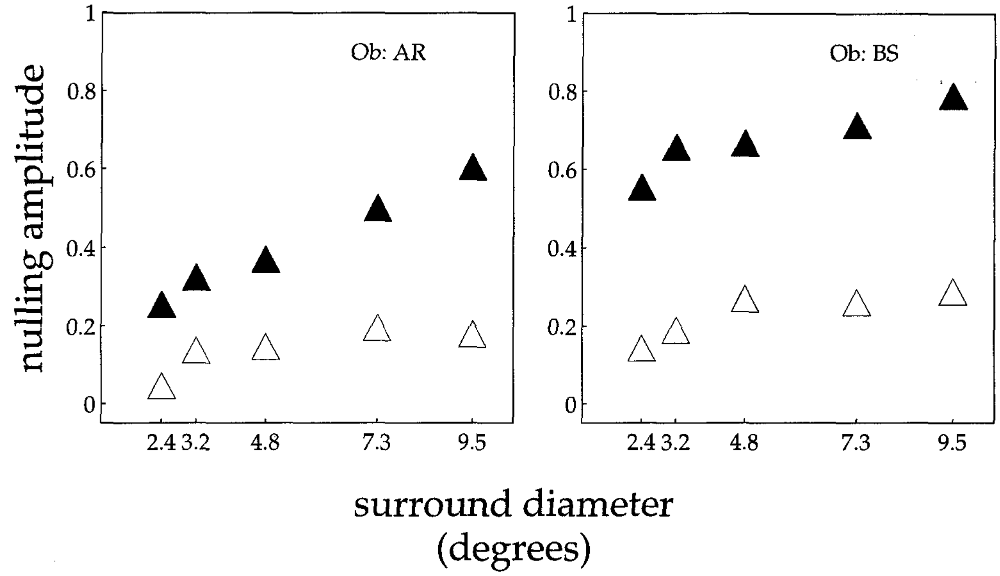

FIGURE 9. Results of Experiment 4 for two observers. The amplitude of modulation required to null induction plotted against the outer radius of the modulating surround annulus. Open symbols are contrast induction nulls and filled symbols are brightness induction nulls.

and $A(\Omega,s)$ is the signed magnitude of the luminance difference between the inducing point at (Ω,s) and the surround mean level.

Although it is clear, from the non-additivity in Experiment 2 and the compression in Experiment 3, that this linear model will produce a qualitatively poor fit to the contrast induction data, examining the fit of this model gives an indication of the type and amount of non-linearity required. In the case of contrast induction, the definitions of the variables in equation (2) are the same as above, except that y is the total induced contrast, and $A(\Omega,s)$ is the difference between the contrast level of the surround at the point (Ω,s) and the mean contrast level of the surround.

The stimuli used in these experiments were circularly symmetric and varied only along radial lines, therefore, if the weighting function is assumed to be isotropic, equation (2) can be reduced to a function of just the radial distance. For a surround consisting of a drifted single sinusoid of spatial frequency equal to ϕ_i c/deg, the induced effect at time t for the center point of the circular test can be expressed as:

$$y(t,\phi_i) = -A\int_L^X g(s)\cos[2\pi(\rho_0 t - \phi_i s + \phi_i L)]s\,ds \quad (3)$$

where A is the amplitude of the surround sine-wave; L is the inner edge of the surround (i.e., the radius of the test disk); X is the outer edge of the surround; and ρ_0 the temporal frequency of the drift (in c/sec). For the present model, given that the test is uniform in contrast and luminance, the induced effect of all points in the test on the test center is zero. Therefore, equation (3) is expressed solely in terms of the effect of the surround. In the case of compound sine-wave stimuli, with a second sinusoid of spatial frequency, ϕ_j c/deg is given by:

$$y(t,\phi_i,\phi_j) = \frac{1}{2}y(t,\phi_i) + \frac{1}{2}y(t,\phi_j) \quad (3a)$$

Since the induced contrast and brightness modulations can be suitably nulled with the addition of real sinusoidal modulation with the same temporal frequency as the inducing modulation (Krauskopf *et al.*, 1986; Zaidi *et al.*, 1991, 1992; Chubb *et al.*, 1989, Singer and D'Zmura, 1994) it is sufficient to describe the inducing, induced, and nulling modulations in terms of their amplitude and phase. For each component, we derived the amplitude and phase of the induced modulation by taking the Fourier transform of equation (3) in the temporal frequency domain. By exploiting the fact that the drift was at a constant velocity given by ρ_0 divided by ϕ_i, the Fourier transform was simplified to equation (4):

$$Y(\rho_0,\phi_i) = -\frac{A}{2}[\delta(\rho-\rho_0) + \delta(\rho+\rho_0)]e^{i2\pi\phi_i L}\int_L^X g(s)e^{i2\pi\phi_i s}s\,ds \quad (4)$$

where $Y(\rho,\phi_i)$ is the Fourier transform of induced modulation for a surround of spatial frequency ϕ_i drifted toward the test point at a temporal frequency of ρ_0, and δ is the Dirac delta function.

If the three assumptions of the model are satisfied, then given the proper choice of $g(s)$, equation (4) should fit the data. Since many smooth monotonic functions can be approximated by exponential functions, it was assumed that the spatial weighting function could be approximated by a negative exponential function of the form:

$$g(s) = \kappa e^{-\alpha s} \quad (5)$$

Equation (5) was substituted into equation (4), and solved to obtain the following expression:

$$Y(\rho_0, \phi_i) = \frac{-A\kappa}{(\alpha + i2\pi\phi_i)^2}((1 + \alpha X + i2\pi\phi_i X)e^{i2\pi\phi_i L - \alpha X - i2\pi\phi_i X} - (1 + \alpha L + i2\pi\phi_i L)e^{-\alpha L}) \quad (6)$$

Expressions for the amplitude and the temporal phase of the induced modulation were then derived by transforming the RHS of equation (6) into the polar form:

$$Y(\rho_0, \phi_i) = AMPLITUDE * e^{iPHASE}. \quad (7)$$

Best fits were found to the compound sinusoid data from Experiment 2 and the amplitude series data from Experiment 3 simultaneously, using the MATLAB "fmins" function which is a standard simplex algorithm for multi-dimensional minimization. For both observers, optimal fits to the 64 paired frequency data from Experiment 2 exhibited the predicted failure of the model to capture the non-linear compression in the contrast induction data. However, this model was able to fit the contours of the brightness induction curves, corroborating the conclusions reached by Zaidi *et al.* (1992).

WEIGHTED SPATIAL INTEGRATION WITH A NON-LINEAR AMPLITUDE FUNCTION

In this section we assume that local contrast signals from each point in the image pass through an amplitude compression in the visual system prior to the stage of lateral interactions responsible for contrast induction. Such a non-linearity will have two effects on the spatial summation model. Inside the surround, the non-linearity will reduce the effective contrast of the surrounding wave. Inside the test, the non-linearity will reduce the effectiveness of the nulling modulation. Mathematically, this is represented by:

$$y = -\zeta[N] = -\int_0^{2\pi} \frac{\int_0^{\infty} g(\Omega, s)\zeta[A(\Omega, s)]sds}{2\pi} d\Omega \quad (8)$$

where ζ is an odd-symmetric non-linear compressive function, y is the actual induced modulation and N is the measured nulling amplitude. We used

$$\zeta[A] = A - cA^3 \quad (9)$$

as the odd symmetric compressive function of amplitude A. In additional computer simulations we found no significant improvements to the fits with the addition of higher order terms.

When applied to sinusoidal stimuli, ζ generates higher order harmonics. However, the optimal choice of the compressive non-linearity for the fits to the present data, generated higher harmonic energy that was less than 1% of the energy in the fundamental. Substituting $\zeta[A]$ and $g(s)$ into the one-dimensional form of equation (8) yields an instantaneous induction level given by:

$$y(t) = -N(t) + cN^3(t) = -\int_X^L \kappa e^{-\alpha s}\left[A(s,t) - cA^3(s,t)\right]sds \quad (10)$$

where $A(s,t)$ is the amplitude at radius s and time t of the surround generated by a sum of spatial sine-waves for Experiment 2, or a single temporal sine-wave for Experiment 3. By using Fourier transforms similar to those used for the analysis of the linear model, and

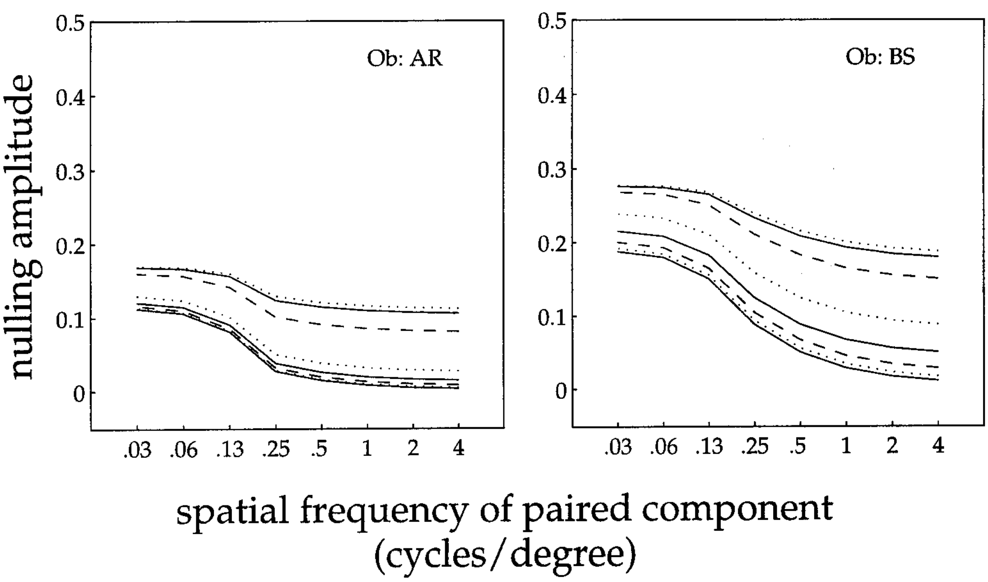

FIGURE 10. Non-linear weighted spatial summation model fit to contrast induction data from Experiment 2, for two observers. With the addition of non-linear compression after spatial summation, the model is able to fit the response compression at the lower spatial frequencies. For key to line types see Fig. 6.

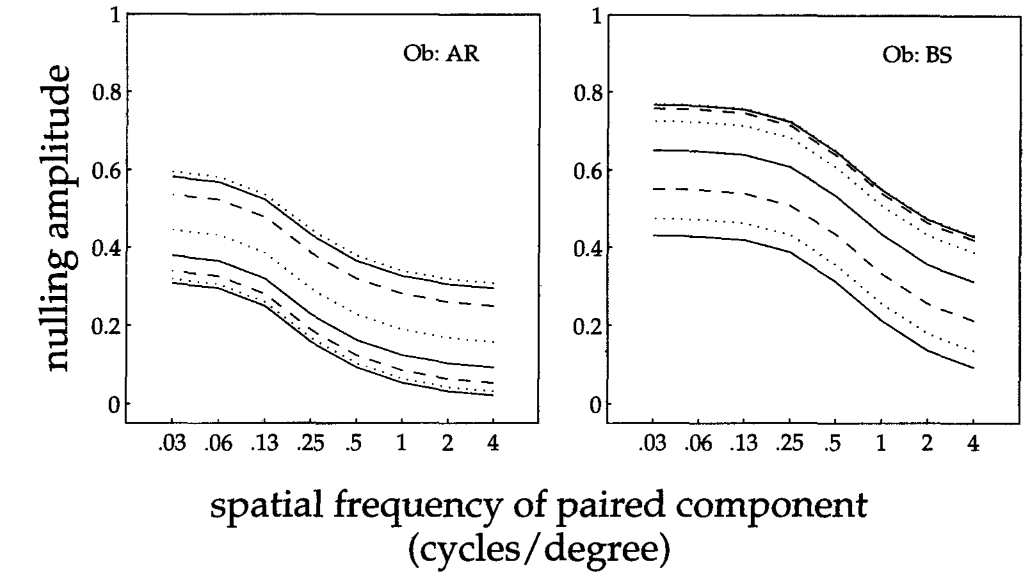

FIGURE 11. Non-linear weighted spatial summation model fit to brightness induction data from Experiment 2, for two observers. For key to line types see Fig. 6.

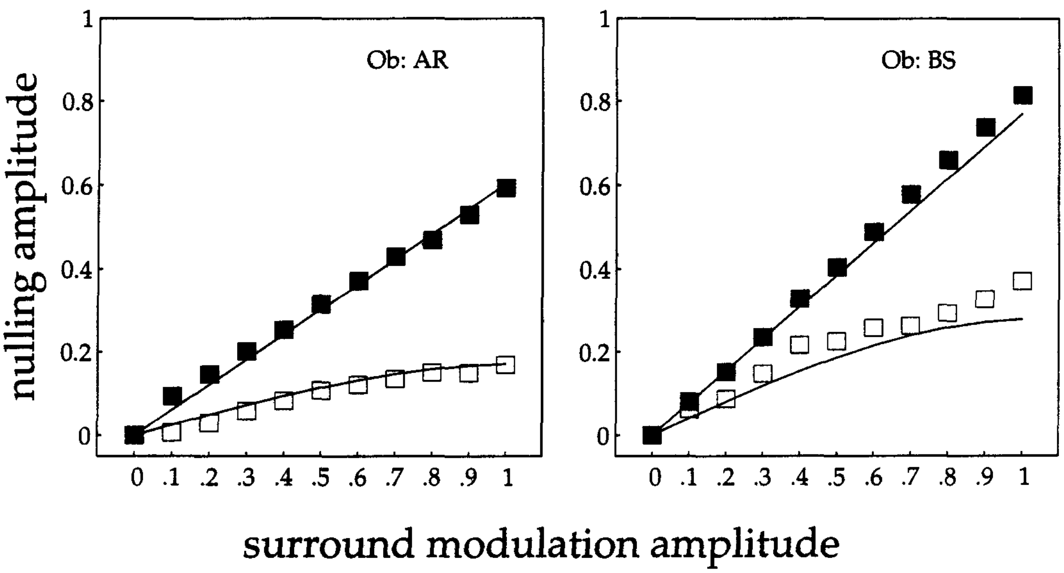

FIGURE 12. Non-linear weighted spatial summation model fit to data from Experiment 3, for two observers. Solid lines are the model fits, open symbols are the contrast nulls and filled symbols are brightness nulls. With non-linear compression, the model is able to fit the contrast response compression that occurs as the inducing amplitude increases.

removing higher-order harmonics, we derived an expression for the amplitude of the inducing stimulus.

Best fits were found to the compound sinusoid data from Experiment 2 and the amplitude series data from Experiment 3 simultaneously. For both observers, optimal fits to the 64 paired frequency contrast induction data from Experiment 2 were able to capture the non-linear compression at the lower frequency levels. As shown by the fits in Figs 10 and 11, the addition of amplitude compression reduces the range covered by the left-hand side of the curves (pairs which include the lowest spatial frequency) compared to the right-hand side (pairs which include the highest spatial frequency). Though the non-linear model does produce a slightly better fit to the brightness induction data, it does not indicate the presence of a compression in the brightness induction system, because the improvement of the fit (compared to the linear model) is limited, and the amount of compression suggested is minimal.

Figure 12 shows the fits to the amplitude variation data from Experiment 3. The extended model is able to capture the compression in the observer's contrast-induction function. For contrast induction the value of c, the compression constant, was 0.15 for AR and 0.37 for BS.

Using the parameters estimated from the fit to Experiments 2 and 3, we generated predictions for the data from Experiment 4. For contrast induction, the

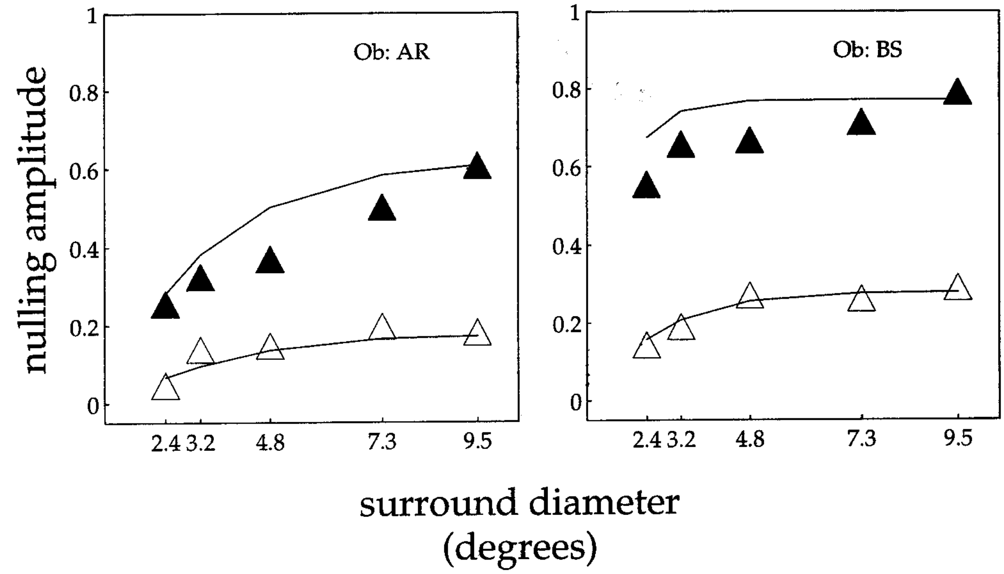

FIGURE 13. Non-linear weighted spatial summation model fit to data from Experiment 4, for two observers. Solid lines are the model fits, open symbols are the contrast nulls and filled symbols are brightness nulls.

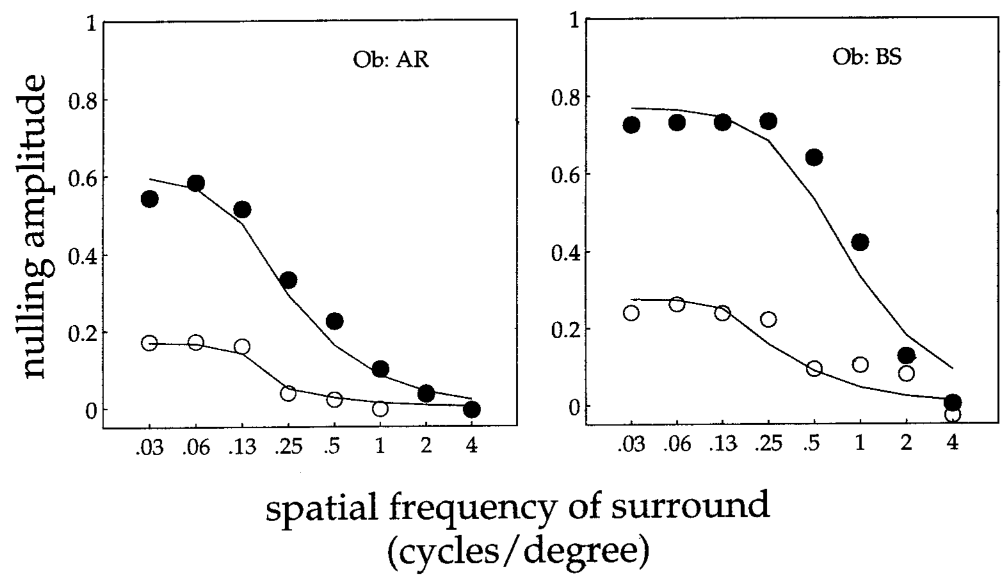

FIGURE 14. Non-linear weighted spatial summation model fit to data from Experiment 1, for two observers. Solid lines are the model fits, open symbols are the contrast nulls and filled symbols are brightness nulls.

extended model predicts curves which are similar to the observed data, as shown in Fig. 13. For the brightness induction data, the predicted curve passes through the highest points for both observers, but the curves do not pass through the points, so the fit deserves further comment. First, brightness induction has been shown to be spatially additive not only in this paper, but also in Zaidi *et al.* (1992) and Spehar *et al.* (1996). If the model is fit solely to the annulus induction data, then a good fit can be obtained with different space constants, but then the model is not optimal for the rest of the data. Second, because the compressive response non-linearity for contrast selectively attenuates the effects of low spatial frequency surrounds, the contrast curves seem to asymptote earlier than the brightness curves, but this may not reflect the relative sizes of space constants. Third, the low frequency asymptotes for brightness and contrast induction in Fig. 14 and Zaidi *et al.* (1992) are more reliable estimates of the spatial extent of brightness and contrast summation than the annulus data, and are reproduced well by the model. For these reasons we do not believe that the model needs to be elaborated for these conditions. Spehar *et al.* (1996) and Zaidi *et al.* (1996) present elaborations of the model for brightness induction where there are differences in mean adaptation level and spatial configurations.

The spatial weighting functions, $e^{-\alpha s}$, for the two observers are shown in Fig. 15. For both observers the contrast function is shallower than the brightness function. Because the surrounding annulus ranges from 0.5 to

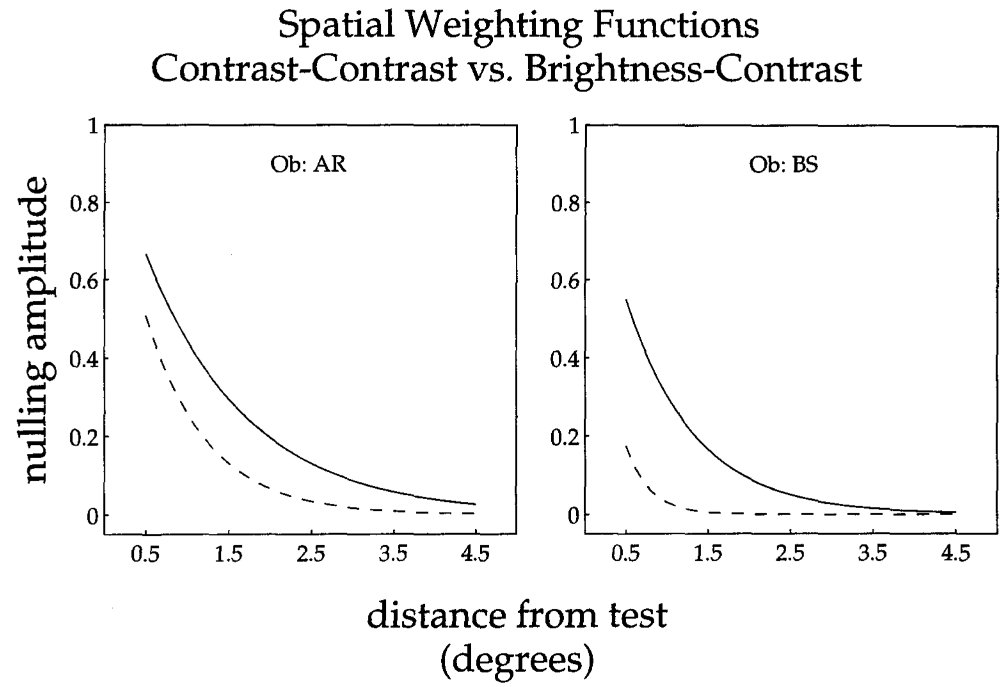

FIGURE 15. Spatial weighting functions from best non-linear model fits to contrast (solid lines) and brightness (dashed lines) induction data. Data shown for two observers.

4.5 deg, we only show the weighting function for this interval; when extrapolated to $s = 0$, each of these weighting functions equals 1. The space constant equal to $1/\alpha$ measured in degrees of visual angle, is equal to the distance from the test at which the effectiveness of a surround point has fallen to $1/e$ of the maximum. The best estimates of the space constants for observer AR were 1.23 and 0.74 for contrast and brightness induction, respectively, and 0.84 and 0.29 for observer BS.

SUMMARY AND DISCUSSION

We have shown that both contrast induction and brightness induction can be explained by a punctate weighted spatial integration model, i.e., the total induced effect is a simple sum of the effects of individual elements of the surround. However, integration of contrast induction, though resulting in a weaker total amount of induction than brightness induction, occurs over a greater distance. This can be seen in the spatial weighting functions shown in Fig. 15. The perceived internal contrast of a test, though less affected by the surround, is influenced by surrounds over a greater distance than is the perceived brightness of the same test.

To model contrast induction, a non-linearity had to be added to the linear model for brightness induction proposed by Zaidi *et al.* (1992). We found that the difference between induced brightness and induced contrast required only the addition of a non-linear amplitude response in the contrast model. Though a slight improvement in modeling brightness induction was also achieved with a compressive model, the best-fitting response function was close to linear, and the improvement in the fit from the linear model was small. The success of the present model suggests that contrast compression occurs in the visual system prior to the lateral interactions that generate induction (Shapley and Victor, 1979). It is interesting that a saturating non-linearity was required for contrast but not for brightness, over the same stimulus luminance levels.

The magnitudes of the modulations required to null brightness induction are in agreement with those found by Zaidi *et al.* (1992). However, there is a significant difference between the magnitudes of contrast-induction in our observations vs those reported by Singer and D'Zmura (1995), who reported induction levels in the range of 5%. We believe this difference is due to the different spatial arrangement used in that study; namely, a 2 deg test disk, compared with the 1 deg test used in the present study. For a 2 deg test, given the contrast spatial weighting functions of our two observers, our model would predict smaller nulling modulation amplitudes, close to those found by Singer and D'Zmura (1995).

The contrast spatial weighting functions estimated in this paper are obviously for textures composed of squares of one particular size. On the basis of their measurements using surrounds of different sizes and at different distances from the test, Cannon and Fullenkamp (1991) have claimed that the space constant for spatial integration decreases with increasing spatial frequency content of the stimuli. We repeated Experiment 1 with textures composed of larger and smaller squares, but the results were inconclusive. For observer AR there was a systematic change across square sizes in the functions relating nulling amplitude to the spatial frequency of the surround contrast sine-wave, and the results could be modeled by decreasing the space constant for increasing square sizes. However, the results could be modeled just as well by scaling the magnitude parameter while keeping the space constants identical. For observer BS there was no systematic effect of changing square size.

The physiological implications of this study would be clearer if the substrates for contrast and brightness induction were better understood. From the results of a number of studies, it is clear that perceived brightness reflects lateral interactions at many stages of the visual system, however, for perceived contrast, far less is known. The space constants estimated in this study can, however, be used as lower bounds on the spatial extents of lateral connections relevant to perceived contrast and brightness. Given the physiologically measured sizes of retinal and cortical receptive fields, the estimated space constants of 0.84 and 0.29 deg for brightness induction make it unlikely that simple center–surround receptive field explanations would suffice. The space constants of 1.23 and 0.74 deg for contrast induction (compare to Cannon and Fullenkamp, 1991; Singer and D'Zmura, 1994) are even more extensive and would be worth comparing to the spatial extent of contrast normalization in the cortex (Solomon *et al.*, 1993; Carandini and Heeger, 1994).

REFERENCES

Adelson, E. H. (1993). Perceptual organization and the judgment of brightness. *Science, 264*, 1333–1336.

Cannon, M. W. & Fullenkamp, S. C. (1991). Spatial interactions in apparent contrast: inhibitory effects among grating patterns of different spatial frequencies, spatial positions and orientations. *Vision Research, 31*, 1985–1998.

Carandini, M. & Heeger, D. J. (1994). Summation and division by neurons in primate visual cortex. *Science, 264*, 1333–1336.

Chevreul, M. E. (1839). *De la loi du contraste simultane des couleurs.* Paris: Pitois-Levreault.

Chubb, C., Sperling, G. & Solomon, J. A. (1989). Texture interactions determine perceived contrast. *Proceedings of the National Academy of Sciences USA, 86*, 9631–9635.

Ejima, Y. & Takahashi, S. (1985). Apparent contrast of a sinusoidal grating in the simultaneous presence of peripheral gratings. *Vision Research, 25*, 1223–1232.

Krauskopf, J., Zaidi, Q. & Mandler, M. B. (1986). Mechanisms of simultaneous color induction. *Journal of the Optical Society of America A, 3*, 1752–1757.

Shapley, R. & Victor, J. D. (1979). The contrast gain control of the cat retina. *Vision Research, 19*, 431–434.

Singer, B. & D'Zmura, M. (1994). Color contrast induction. *Vision Research, 34*, 3111–3126.

Singer, B. & D'Zmura, M. (1995). Contrast gain control: a bilinear model for chromatic selectivity. *Journal of the Optical Society of America A, 12*, 667–685.

Solomon, J. A., Sperling, G. & Chubb, C. (1993). The lateral inhibition of perceived contrast is indifferent to on-center/off-center segregations, but specific to orientation. *Vision Research, 33*, 2671–2683.

Spehar, B., De Bonet, J. S. & Zaidi, Q. (1996). Brightness induction from uniform and complex surrounds: a general model. *Vision Research, 36*, 1893–1906.

Zaidi, Q. & Sachtler, W. (1991). Motion adaptation from surrounding stimuli. *Perception, 20*, 703–714.

Zaidi, Q., Spehar, B. and Shy, M. (1996). Induced effects of backgrounds and foregrounds in three-dimensional configurations: the role of T junctions. *Perception*, in press.

Zaidi, Q., Yoshimi, B. & Flanigan, N. (1991). The influence of shape and perimeter length on induced color contrast. *Journal of the Optical Society of America A, 8*, 1810–1817.

Zaidi, Q., Yoshimi, B., Flanigan, N. & Canova, A. (1992). Lateral interactions within color mechanisms in simultaneous induced contrast. *Vision Research, 32*, 1695–1707.

Acknowledgements—Portions of this work were presented at ARVO 1994. We would like to thank Alix Rosenstein and Branka Spehar for making careful and patient observations. Some of this work was conducted when the authors were at Columbia University and the Lighthouse, NY. This work was partially funded by NEI grant EY07556 to Q. Zaidi.